Journal of Molecular Liquids 334 (2021) 116070

Contents lists available at ScienceDirect

Journal of Molecular Liquids

journal homepage: www.elsevier.com/locate/molliq

Inclusion complexes of cannabidiol with β-cyclodextrin and its derivative: Physicochemical properties, water solubility, and antioxidant activity

Hang Li [a,b], Sen-Lin Chang [a,b], Tan-Ran Chang [a,b], Ying You [a], Xiao-Dong Wang [a], Li-Wei Wang [a], Xiao-Fan Yuan [a], Ming-Hui Tan [a,b], Pei-Dong Wang [a,b], Peng-Wei Xu [a,b], Wei-Bo Gao [c], Qing-Sheng Zhao [a,*], Bing Zhao [a,*]

[a] Division of Bioresources and Health Product Engineering, State Key Laboratory of Biochemical Engineering, Institute of Process Engineering, Chinese Academy of Sciences, Beijing 100190, China
[b] School of Chemical Engineering, University of Chinese Academy of Sciences, Beijing 100049, China
[c] Yunnan Hempmon Pharmaceutical Co., Ltd, Kunming 650032, China

ARTICLE INFO

Article history:
Received 9 January 2021
Revised 11 March 2021
Accepted 4 April 2021
Available online 8 April 2021

Keywords:
Cannabis sativa L.
Cannabidiol
2, 6-di-O-methyl-β-cyclodextrin
Inclusion complex
Water solubility
Antioxidant activity

ABSTRACT

Cannabidiol (CBD), which has a wide variety of biological activities, is one of the phytocannabinoids from *Cannabis sativa* L. However, due to the poor aqueous solubility, its applications in food, cosmetic, and pharmaceutical fields are limited. Moreover, the previous researches on the improvement in the solubility of CBD are rare. Cyclodextrins (CDs) are useful materials to improve the solubility of poorly water-soluble molecules. Therefore, this work was aimed to study the physicochemical properties, water solubility, and dissolution rate of the inclusion complexes of CBD with β-cyclodextrin (β-CD) and 2, 6-di-O-methyl-β-cyclodextrin (DM-β-CD), and to determine the influence of complexation on the antioxidant activity of CBD. Job's plot and phase solubility study revealed that CBD formed inclusion complexes with β-CD and DM-β-CD at a 1:1 stoichiometric ratio. The thermodynamics analysis demonstrated that the inclusion process was spontaneous and endothermic. Then, the inclusion complexes of CBD with β-CD or DM-β-CD were prepared and characterized by PXRD, FT-IR, DSC, SEM, and ^{1}H NMR. The loading efficiency (LE) of the two inclusion complexes was 20.4% and 17.7% respectively, while the complexation efficiency (CE) was 92.4% and 90.8% respectively. Moreover, the results of molecular docking further showed that CBD was encapsulated successfully. The results also displayed that the water solubility of CBD in CBD/β-CD inclusion complex (IC) and CBD/DM-β-CD IC was significantly increased to 0.395 and 14.118 μg/mL, which was enhanced by 17-fold and 614-fold respectively at such a high LE, and the in vitro dissolution rate of CBD was also promoted after complexation. Besides, the antioxidant activity of CBD was improved after encapsulation with β-CD and DM-β-CD. Significantly, the ABTS free radical scavenging ability of the two inclusion complexes was better than that of Vitamin C (Vc).

Abbreviations: CBD, Cannabidiol; CDs, Cyclodextrins; β-CD, β-cyclodextrin; DM-β-CD, 2 6-di-O-methyl-β-cyclodextrin; IC, Inclusion complex; THC, tetrahydrocannabinol; FDA, Food and Drug Administration; BCS, Biopharmaceutical classification system; α-CD, α-cyclodextrin; γ-CD, γ-cyclodextrin; FT-IR, Fourier transform infrared spectroscopy; PXRD, Powder X-ray diffraction; DSC, Differential scanning calorimetry; SEM, Scanning electron microscopy; NMR, Nuclear magnetic resonance; ABTS, 2 2′-azinabis (3-ethyl-benzothiazoline-6-sulfonic acid) diammonium salt; DPPH, 1 1-diphenyl-2-picrylhydrazyl; HPLC, High performance liquid chromatography; Abs, Absorbance; CE, Complexation efficiency; LE, Loading efficiency; TMS, Tetramethylsilane; EC_{50}, 50% effective concentration; PM, Physical mixture; Vc, Vitamin C.

* Corresponding authors at: 1 North 2nd Street, Zhongguancun, Haidian District, Beijing, China.
E-mail addresses: lihang18@mails.ucas.edu.cn (H. Li), changsenlin14@mails.ucas.edu.cn (S.-L. Chang), changtanran@163.com (T.-R. Chang), youy_0922@163.com (Y. You), xdwang@ipe.ac.cn (X.-D. Wang), lwwang@ipe.ac.cn (L.-W. Wang), xfyuan@ipe.ac.cn (X.-F. Yuan), mhtan@ipe.ac.cn (M.-H. Tan), wangpeidong19@mails.ucas.edu.cn (P.-D. Wang), xupengwei17@mails.ucas.edu.cn (P.-W. Xu), simon.gao@hempmon.com (W.-B. Gao), qszhao@ipe.ac.cn (Q.-S. Zhao), bzhao@ipe.ac.cn (B. Zhao).

https://doi.org/10.1016/j.molliq.2021.116070
0167-7322/

1. Introduction

Cannabis sativa L. (hemp) has many kinds of phytocannabinoid compounds, including cannabidiol (CBD, Fig. 1), which is the second most abundant cannabinoid after tetrahydrocannabinol (THC) [1]. It is noteworthy that CBD has no psychotropic activity, but THC can cause psychoactive side effects [2,3]. CBD has been demonstrated to possess a wide variety of biological activities, including antioxidative [4], antibacterial [5], anticancer [6–8], anti-inflammatory [9], antidepressant-like [10], hepatoprotective [11], anti-radiation [12], neuroprotective [13], antipsychotic [14–16], antiepileptic [17], antidiabetic [18], immunoregulatory [19] and so on. Therefore, CBD has immense applied value in functional foods, cosmetic, nutraceutical, and pharmaceutical products. Epidiolex®, a pharmaceutical preparation of CBD was approved by the US Food and Drug Administration (FDA) in 2018 for seizures treatment [20]. However, CBD is a biopharmaceutical classification system (BCS) class II drug, indicating that the aqueous solubility of CBD is very poor, which leads to low oral bioavailability. So it is urgent to explore an effective strategy for increasing the water solubility of CBD for its development and application in many fields.

Cyclodextrins (CDs, Fig. 2) are circular table-shaped cyclic oligosaccharides and composed of glucopyranose units linked by α-1, 4-glycosidic bonds [21]. The outer surface of CDs is hydrophilic while the inner cavity which can accommodate insoluble molecules is hydrophobic. CDs are often used to improve the water solubility and chemical stability of biologically active natural products, such as rosmarinic acid [22], resveratrol [23], quercetin [24], betulin [25], and curcumin [26]. β-cyclodextrin (β-CD, Fig. 2) is one of the most widely used CDs because its cavity is compatible with common guests with molecular weights between 200 and 800 g/mol [27]. Lv et al. [28] prepared the inclusion complex (IC) of CBD with β-CD by suspension method, claiming that the water solubility of CBD was improved but the data of loading rate was not presented. Mannila et al. [29] also used β-CD as a drug carrier to enhance the absorption of CBD in rabbits by sublingual administration. However, the water solubility of unmodified β-CD is bad. Furthermore, it could not be used safely because of its nephrotoxicity [30]. Thus, some substituted β-CD have been obtained through different chemical modifications and used in medicine, food, and cosmetic industries, including 2, 6-di-O-methyl-β-cyclodextrin (DM-β-CD, Fig. 2), which is made by methylation of the hydroxyl groups at C2 and C6 of all glucose units of β-CD. DM-β-CD has gained tremendous attention owing to its relatively flexible cavity size, higher water solubility, low toxicity, and better inclusion capability [31]. Because of these advantages, DM-β-CD shows a better potential to be applied than β-CD. Wu et al. [32] reported that DM-β-CD possessed higher apparent stability constant than β-CD with 2R, 3R-dihydromyricetin, indicating that the cavity size of DM-β-CD was more suitable. Dong et al. [33] also illustrated that quercetin/DM-β-CD IC had significantly enhanced dissolution rate and thermal stability compared with those of quercetin/β-CD IC.

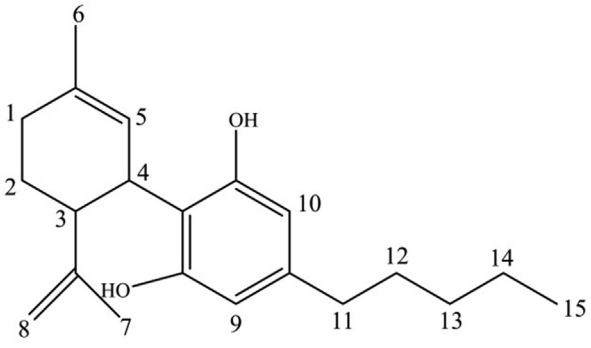

Fig. 1. The chemical structure of CBD.

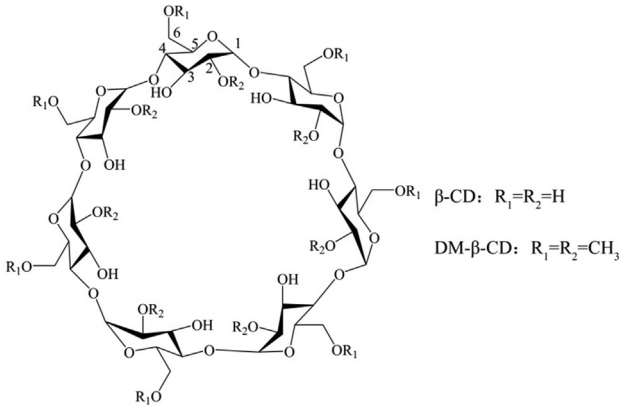

Fig. 2. The chemical structures of CDs.

Although several studies about the inclusion complexes of CBD with CDs have been reported as mentioned above, to the best of our knowledge there is no article concerning the encapsulation of CBD with DM-β-CD up to now. Meanwhile, the changes of biological activities before and after inclusion are still unclear. Therefore, the present work was aimed to elucidate the binding behavior between CBD and DM-β-CD or β-CD, and to evaluate the water solubility, dissolution performance, and antioxidant activity of CBD/DM-β-CD IC and CBD/β-CD IC. First of all, we compared the inclusion ability of several CDs, including α-cyclodextrin (α-CD), β-CD, γ-cyclodextrin (γ-CD), and DM-β-CD. Then the two inclusion complexes, CBD/DM-β-CD IC and CBD/β-CD IC which exhibited strong interactions, were prepared, characterized, and investigated. The structural and thermal properties were analyzed by Fourier transform infrared spectroscopy (FT-IR), powder X-ray diffraction (PXRD), differential scanning calorimetry (DSC), scanning electron microscopy (SEM), and nuclear magnetic resonance (NMR). In addition to the experimental analysis, molecular docking was employed to estimate the most possible modes and the binding energy of the combination between CBD and CDs. Furthermore, the water solubility and in vitro dissolution rate of the inclusion complexes were assessed to verify the solubility enhancement of CBD. Finally, antioxidant activity tests based on free radical scavenging assay were carried out to evaluate the effect of inclusion on the antioxidant activity of CBD.

2. Materials and methods

2.1. Materials

CBD (98%, $M_W \approx 314$) was supplied by Yunnan Hempmon Pharmaceutical Co., Ltd. (Yunnan, China). α-CD (98%, $M_W \approx 973$), β-CD (98%, $M_W \approx 1135$), γ-CD (98%, $M_W \approx 1297$), DM-β-CD (98%, $M_W \approx 1331$), and 2, 2′-azinabis (3-ethyl-benzothiazoline-6-sulfonic acid) diammonium salt (ABTS, 98%) were purchased from Shanghai Aladdin Biochemical Technology Co., Ltd. (Shanghai, China). 1, 1-diphenyl-2-picrylhydrazyl (DPPH, 96%) was obtained from Shanghai Macklin Biochemical Technology Co., Ltd. (Shanghai, China). Solvents used in high performance liquid chromatography (HPLC) analysis were of chromatographic grade. Other reagents, which were of analytical grade, were purchased from Sinopharm Chemical Reagents Co., Ltd. (Shanghai, China). Deionized water was used during the whole experiment process.

2.2. HPLC analysis

The HPLC (1260 Infinity, Agilent Technology, Palo Alto, USA) system equipped with a UV/Vis detector was used to quantify CBD. The HPLC analytical conditions were achieved on a MultoHigh 100 RP18-3μ (125 mm × 4.6 mm) column (CS-Chromatographie-Service GmbH, Langerwehe, Germany) with a mobile phase containing methanol and water in the ratio (87:13, v/v). The flow rate was 0.2 mL/min. The column temperature was maintained at 35 °C. The wavelength detected was 220 nm and the volume of each injection was 10 μL. All the samples were filtered through a 0.22 μm membrane filter before being analyzed.

2.3. Phase solubility study

Phase solubility study for the CBD/CDs system was carried out following the method described by Higuchi and Connors [34]. An excess amount of CBD was added into a conical flask containing 10 mL of an aqueous solution of α-CD, β-CD, γ-CD, or DM-β-CD at various concentrations ranging from 0 to 24 mM. The conical flask was shaken at 30℃ for 24 h in a constant temperature incubator shaker. Then the suspension was centrifuged at 4,000 rpm for 10 min and the supernatant was filtered through a 0.22 μm membrane filter. Next, the amount of CBD dissolved was evaluated by HPLC. Phase solubility diagram was obtained by plotting concentration of CBD *vs* concentration of CD. And the apparent stability constant (K_S) of each CD was calculated from the slope of the phase solubility diagram according to the following equation (Eq. (1)).

$$K_S = slope/[S_0(1 - slope)] \quad (1)$$

where S_0 (2.3×10^{-2} μg/mL) is the original solubility of CBD in water.

2.4. Job's plot

Job's plot, as a technique of continuous variation, is commonly used for determining the stoichiometry of inclusion [35]. Briefly, equimolar (2×10^{-4} M) CBD and CD (β-CD or DM-β-CD) in methanol–water solutions (55:45, v/v) were mixed to a constant volume (1 mL: 9 mL; 2 mL: 8 mL; 3 mL: 7 mL and so on). After stirring for 1 h at 30 °C, the sample vials were centrifuged at 4,000 rpm for 10 min. The absorbance (Abs) of each solution was measured by UV/Vis spectroscopy (UV-2802, Unico Instrument, Calabasas, USA) at 220 nm and ΔAbs was determined as the difference between Abs with and without CDs. Then, the Job's plot was obtained by plotting ΔAbs × R *vs* R (calculated by Eq. (2)).

$$R = \frac{[CBD]}{[CBD] + [CD]} \quad (2)$$

2.5. Determination of thermodynamic parameters

According to the phase solubility diagrams of 30, 40, 50, 60 ± 0.5 °C, the thermodynamic parameters of the encapsulation process, ΔG^0, ΔH^0, and ΔS^0 were calculated from the Gibbs and Van't Hoff equation.

$$\Delta G^0 = -RT \times \ln K_S \quad (3)$$

$$\ln K_S = -\Delta H^0/RT + \Delta S^0/R \quad (4)$$

where T represents temperature, R is the universal gas constant about 8.314 J/(mol·K), ΔH^0 and ΔS^0 are standard enthalpy change and entropy change, respectively, ΔG^0 refers to Gibbs free energy change.

For a linear regression curve of $\ln K_S$ *vs* 1/T, $-\Delta H^0/R$ and $\Delta S^0/R$ play a role as slope and intercept, respectively.

2.6. Preparation of inclusion complexes and physical mixtures

CBD/β-CD IC and CBD/DM-β-CD IC were prepared by freeze-drying method. The following technological parameters were determined by optimization. Briefly, CBD and CD were exactly weighted in a molar ratio of 1:1. CD (β-CD or DM-β-CD, 4×10^{-2} mmol) was solubilized in 40 mL of 40% ethanol, being stirred completely for 20 min. CBD (4×10^{-2} mmol) was dissolved in 500 μL of ethanol and the obtained solution was added into CD solution slowly. The resulting mixture was magnetically stirred at 30 °C for 6 h, and then filtered through a 0.22 μm membrane. Finally, the filtrate was lyophilized for 2 days by a vacuum freeze drier (LGJ-10E, Beijing SiHuan Scientific Instrument, Beijing, China).

To prepare physical mixtures, CBD and CD were uniformly mixed in a molar ratio of 1:1 using a mortar at room temperature for 5 min. The physical mixtures were placed in a dryer for use.

2.7. Complexation efficiency (CE) and loading efficiency (LE) of CBD in the inclusion complexes

HPLC analysis was used to determine the CBD content in the complexes. In brief, 10 mg of IC was dissolved in 10 mL of methanol, then the obtained solution was treated with ultrasonic processing at room temperature for 40 min to allow enough time for all CBD entrapped to release into the solution. Subsequently, the sample was centrifuged at 4000 rpm for 5 min and the supernatant was analyzed by HPLC. The CE and LE were calculated by Eq. (5) and Eq. (6), respectively.

$$CE(\%) = (M_E/M_T) \times 100 \quad (5)$$

$$LE(\%) = [M_E/(M_E + M_C)] \times 100 \quad (6)$$

where M_E refers to the mass of CBD entrapped, M_T is the total weight of CBD added initially, and M_C represents the weight of CD.

2.8. Characterization of CBD, CDs, physical mixtures, and inclusion complexes

2.8.1. PXRD analysis

The PXRD patterns were collected on an Empyrean X-ray diffractometer (PANalytical B. V., Almelo, Netherlands) equipped with a Cu Kα (λ = 1.5406 Å) radiation source and operated at 40 kV/40 mA. The diffraction data were obtained at 2θ diffraction angles between 5° and 90° with a step size of 0.02626°.

2.8.2. FT-IR analysis

Each sample was adequately mixed with a suitable amount of KBr, and then the mixture was compressed into a tablet before testing. FT-IR spectra were recorded with a Nicolet iS50 FT-IR spectrophotometer (Thermo Fisher Scientific, Madison, USA) between 4000 cm^{-1} and 400 cm^{-1} at an optical resolution of 4 cm^{-1}.

2.8.3. DSC analysis

DSC analysis was carried out on a STA449F3 simultaneous thermal analyzer (Netzsch, Bavaria, Germany). Each sample (5–10 mg) was heated at a rate of 10 °C/min from 30 to 300 °C under a flowing argon atmosphere (flow rate: 20 mL/min) in an aluminum pan.

2.8.4. SEM analysis

The surface morphology of each sample was observed by a JSM-6700F field emission scanning electron microscope (JEOL, Tokyo, Japan). Before observing, the samples were evenly fixed on a brass stub using double-sided adhesive tape, and then coated by gold

sputter, they were made to be electrically conductive. Subsequently, the images were taken.

2.8.5. ^{1}H NMR analysis

^{1}H NMR experiment was conducted on an AVANCE III spectrometer (600 MHz, Bruker BioSpin, Switzerland) at 25 °C. DMSO d_6 was used as the solvent for all samples. The chemical shift was presented as ppm, tetramethylsilane (TMS) as the internal standard.

2.9. Molecular docking

AutoDock 4.2 software (Scripps Research Institute, La Jolla, USA), a popular and free application for molecular modeling [36], was used in this work to predict the most dominant conformation of the inclusion complexes. The structure of CBD was drawn using ChemBioDraw Ultra 15.0 software (CambridgeSoft, Cambridge, USA), and then optimized by Chem3D Ultra 15.0 (CambridgeSoft, Cambridge, USA) based on the MM2 molecular force field. The structure of β-CD was obtained from the Protein Data Bank (PDB ID: 1z0n) while DM-β-CD was acquired by adding dimethyl to β-CD. The spatial structures of the CDs were also treated by the MM2 method in Chem3D Ultra 15.0. All the nonpolar hydrogen atoms were made to expose. AutoDockTools 1.5.6 was used to add the gasteiger charges for each atom of the abovementioned molecules and AutoGrid 4.2 was employed to estimate the grid maps before molecular docking. With the preparations being completed, docking of CBD with CDs was performed using the Lamarckian genetic algorithm through AutoDockTools.

2.10. Water solubility study

To determine water solubility, an excess amount (equivalent to 10 mg raw CBD) of each sample was suspended in a conical flask containing 20 mL of deionized water and kept for magnetically stirring with a speed of 100 rpm for 24 h at 37 °C. Then the suspension was centrifuged at 4000 rpm for 5 min. The supernatant was analyzed by HPLC.

2.11. In vitro dissolution study

For in vitro dissolution experiment, deionized water was used as the dissolution medium. Each sample (equivalent to 1.5 mg raw CBD) was added into 100 mL of deionized water. The conical flask containing the suspension was magnetically stirred (100 rpm) at 37 °C. At different time intervals (0, 5, 10, 15, 20, 30, 45, 60, 90, 120, 180, 240, 360, 480, 720, 1440 min), aliquot (2 mL) was withdrawn and analyzed by HPLC. At the same time, 2 mL of deionized water was added into the conical flask for maintaining the initial volume of the dissolution medium.

2.12. Antioxidant activity study

2.12.1. ABTS free radical scavenging activity

The ABTS free radical scavenging capacity of CBD, CDs, physical mixtures, and inclusion complexes was evaluated based on a previous method with minor modifications [37]. In brief, 50 mL methanol solution of ABTS (7 mM) was mixed with 880 μL aqueous solution of potassium persulfate (140 mM). The obtained mixture was kept in the dark for 24 h at room temperature. The prepared ABTS stock solution was diluted about 80 times with methanol until the Abs reached 0.70 ± 0.02 at 734 nm. As a result, the ABTS work solution was obtained. Then, 4 mL of ABTS work solution was added into 1 mL of the sample solution of various concentrations. The obtained solution was shaken quickly for 30 s and placed in the dark for another 6 min. Subsequently, the Abs at 734 nm was measured by UV/Vis spectroscopy, and Vitamin C (Vc) was used as a positive control. The scavenging rate of each sample, expressed as SA (%), was calculated with Eq. (7). The 50% effective concentration (EC_{50}) of the samples was speculated by plotting SA (%) *vs* concentration of each sample.

$$ABTS\ SA\ (\%) = \left[1 - \frac{A_{sample} - A_{control}}{A_{blank}}\right] \times 100\% \quad (7)$$

where A_{sample} is the absorbance of the reaction system (ABTS with the sample), $A_{control}$ represents the absorbance of the sample background (methanol with the sample), and A_{blank} refers to the absorbance of the negative control (ABTS with methanol).

2.12.2. DPPH free radical scavenging activity

The DPPH free radical scavenging capacity of CBD, CDs, physical mixtures, and inclusion complexes was assessed according to a reported method with some modifications [38]. Briefly, 100 mL methanol solution of DPPH (0.2 mM) was prepared. Subsequently, 2 mL of DPPH solution was added into 2 mL of the sample solution of various concentrations. The mixture was shaken sufficiently and incubated for 30 min. Finally, the Abs at 517 nm was measured by UV/Vis spectroscopy, and Vc was used as a positive control. The scavenging rate of each sample, expressed as SA (%), was counted using Eq. (8). The EC_{50} value of the samples was determined by plotting SA (%) *vs* concentration of each sample.

$$DPPH\ SA\ (\%) = \left[1 - \frac{A_{sample} - A_{control}}{A_{blank}}\right] \times 100\% \quad (8)$$

where A_{sample} represents the absorbance of the reaction system (DPPH with the sample), $A_{control}$ refers to the absorbance of the sample background (methanol with the sample), and A_{blank} is the absorbance of the negative control (DPPH with methanol).

3. Results and discussions

3.1. Phase solubility study

The phase solubility diagrams of CBD with α-CD, β-CD, γ-CD, and DM-β-CD in water at 30 °C were shown in Fig. 3. The phase solubility analysis is an essential and extensively used technique to estimate the influence of CDs on the solubility of poorly water-soluble molecules, the stoichiometric proportion, and the apparent stability of inclusion complexes [39]. As indicated by the diagrams, the aqueous solubility of CBD increased linearly with the increasing concentration of CDs within the designed concentration range, other than α-CD. Therefore, the three linear phase solubility diagrams can be classified as A_L type diagram based on the definition of Higuchi and Connors, suggesting that the formation of 1:1 complexes between CBD and the three CDs. However, as the concentration of α-CD rose, the water solubility of CBD increased faster, showing a non-linear correlation, which indicated an A_P type phase solubility performance. It demonstrated that the 1:1 and 1:2 CBD/α-CD IC both existed. The order of the calculated K_S (M^{-1}) of the four CBD/CDs was: DM-β-CD (3227.1) > β-CD (315.4) > α-CD (126.5) > γ-CD (26.8). Just as we predicted, β-CD and its derivative exhibited better inclusion ability. The lower K_S of α-CD and γ-CD were probably due to their unsuitable cavity size, which prevented CBD molecule from entering the cavity of α-CD [40] or was too big for CBD to interact effectively with γ-CD, respectively. On the other hand, the K_S of DM-β-CD was higher than that of β-CD, suggesting that the dimethyl substituent can improve the inclusion ability by enlarging the hydrophobic cavity of β-CD or enhancing a hydrogen bonding impact [41]. In consideration of the excellent inclusion ability, β-CD and DM-β-CD were employed in subsequent experiments.

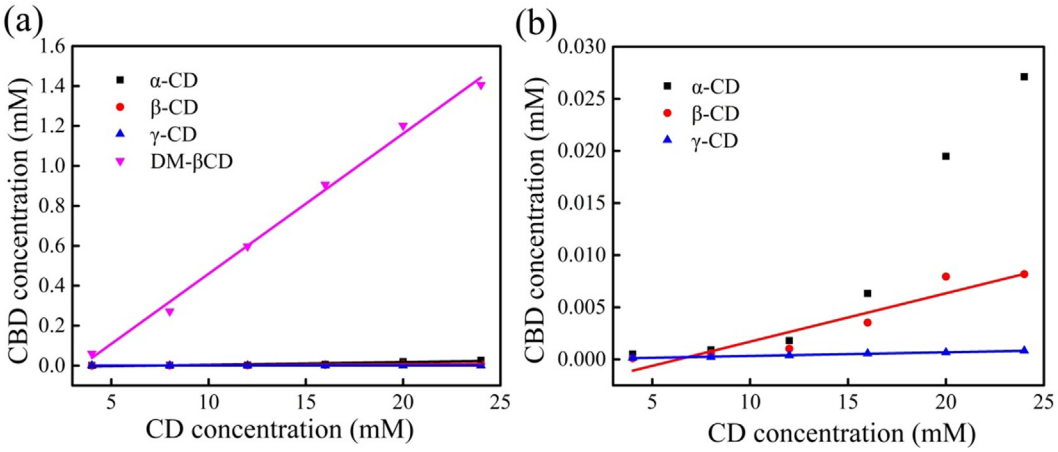

Fig. 3. Phase solubility diagrams of CBD with various CDs at 30 °C in aqueous solution ((b) is a partial enlargement of (a)).

3.2. Job's plot

Job's experiment was achieved to further validate the stoichiometric ratio of the inclusion complexes. Fig. 4 represented the Job's plots of CBD/β-CD IC and CBD/DM-β-CD IC. On the basis of this method, the value of R relevant to the maximum value of ΔAbs × R is considered to be the stoichiometric proportion of the IC. The results showed that the peak values of ordinate appeared at 0.5, indicating that the stoichiometric ratio of the two inclusion complexes was 1:1, which was consistent with the conclusion of the phase solubility study. Therefore, the inclusion complexes were prepared in a 1:1 ratio.

3.3. Thermodynamics analysis

The thermodynamic parameters of the interaction of CBD with CDs were exhibited in Table 1. ΔG^0 was calculated by Eq. (3) after the value of K_S at different temperatures being obtained. ΔH^0 and ΔS^0, which were associated with the slope and intercept of Eq. (4) respectively, were got from the linear regression curves of $\ln K_S$ *vs* 1/T (data not shown in the article). As shown in Table 1, the value of ΔG^0 for the two CDs at all temperatures was negative while the values of ΔH^0 and ΔS^0 were positive, indicating that the complexation processes between CBD and the two CDs were spontaneous and endothermic. Moreover, the encapsulation increased the translational and rotational degrees of freedom of the inclusion complexes instead of making a more ordered system [42]. Based on the second law of thermodynamics, the positive value of ΔH^0 was a major obstacle for the reaction, but its adverse effect was counteracted by ΔS^0, which was more dominant in the complexation processes between CBD and the two CDs [43]. Meanwhile, the values of the thermodynamic parameters during the processes were less than those of the general chemical reactions, suggesting that there were intermolecular hydrogen bonds and Van der Waals force, but no covalent bond [44]. Besides, the thermodynamic parameters of CBD with the two CDs were distinctly different. The absolute value of ΔH^0 and ΔS^0 of CBD with DM-β-CD was less than those with β-CD, while the absolute value of ΔG^0 was greater. The phenomenon indicated a milder endothermic reaction, a less disordered system, and a larger tendency to form a complex in the inclusion process with DM-β-CD. It could be speculated that the larger and more hydrophobic cavity of DM-β-CD played an important role, compared with that of β-CD.

3.4. Complexation efficiency and loading efficiency

CE and LE are two important parameters, which are commonly used to determine the amount of guest molecule entrapped into the cavity of CDs [45]. Based on Eq. (5) and Eq. (6), it can be determined that LE has a positive correlation with CE. Table 2 represented the CE and LE of the two inclusion complexes. For CBD/β-CD IC, the CE and LE were 92.4 ± 0.49% (n = 3) and 20.4 ± 0.53% (n = 3), respectively. For CBD/DM-β-CD IC, they were 90.8 ± 0.34% (n = 3) and 17.7 ± 0.69% (n = 3), respectively. The values of CE of the two complexes were more than 90%, indicating that almost all CBD molecules were entrapped. The high values of CE and LE

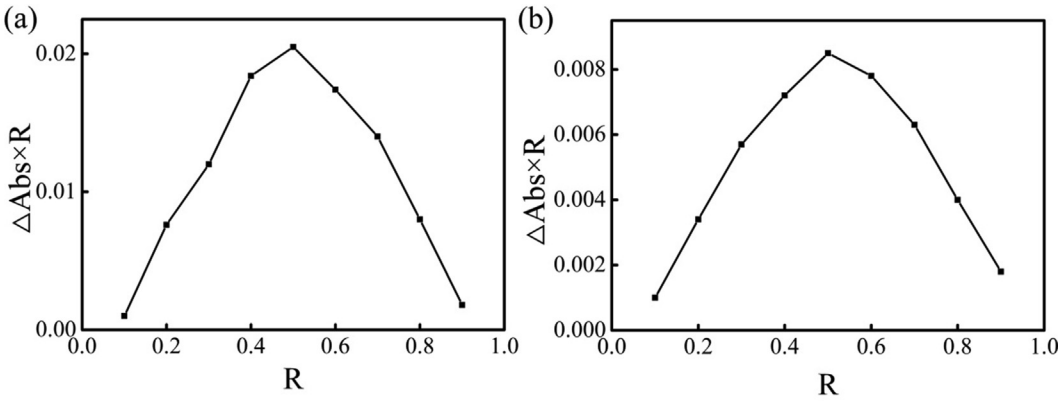

Fig. 4. Job's plots of (a) CBD/β-CD IC and (b) CBD/DM-β-CD IC in 55% methanol at 30 °C.

Table 1
Thermodynamic parameters for CBD/β-CD IC and CBD/DM-β-CD IC at different temperatures.

	ΔG^0 (kJ/mol)		ΔH^0 (kJ/mol)		ΔS^0 (J/mol·K)	
T (°C)	β-CD	DM-β-CD	β-CD	DM-β-CD	β-CD	DM-β-CD
30	−22.26 ± 0.13	−34.90 ± 0.21	81.40 ± 4.54	2.99 ± 0.14	337.98 ± 19.31	125.23 ± 9.49
40	−23.87 ± 0.37	−36.33 ± 0.83				
50	−24.99 ± 0.75	−37.51 ± 1.64				
60	−33.43 ± 0.51	−38.67 ± 1.11				

Results were listed as mean ± SD (n = 3).

Table 2
Complexation efficiency and loading efficiency of CBD/β-CD IC and CBD/DM-β-CD IC.

	CE (%)	LE (%)
CBD/β-CD IC	92.4 ± 0.49	20.4 ± 0.53
CBD/DM-β-CD IC	90.8 ± 0.34	17.7 ± 0.69

Results were listed as mean ± SD (n = 3).

can be attributed to the physicochemical properties and chemical structure of the two CDs. In subsequent experiments, several techniques were adopted to verify that CBD was entrapped into the cavity of CDs successfully.

3.5. Characterization of CBD, CDs, physical mixtures, and inclusion complexes

3.5.1. PXRD analysis

PXRD is an effective method to verify the formation of inclusion complexes with CDs [46]. As shown in Fig. 5, the PXRD pattern of CBD exhibited several sharp characteristic diffraction peaks at 2θ angles of 10.11°, 17.28°, 18.72°, 20.43°, 21.53°, and 22.03°, which showed a high degree of crystallinity of CBD. Similarly, β-CD also displayed many diffraction peaks because of its crystalline state and the diffraction peak at 12.55° was the sharpest. By contrast, DM-β-CD showed almost no characteristic peak due to its amorphous nature. The diffractograms of the physical mixtures were a simple superposition of the diffraction patterns of CBD and CDs. However, compared with the spectra of CBD, CDs, and physical mixtures, the spectra of the inclusion complexes were substantially different. In the diffractogram of CBD/β-CD IC, the characteristic sharp peaks of CBD and β-CD almost disappeared completely while a few new peaks emerged, suggesting the formation of a new crystalline structure. In the diffractogram of CBD/DM-β-CD IC, the diffraction peaks of CBD could not be observed, indicating that the crystalline nature of CBD was destroyed and the state of CBD/DM-β-CD IC was disordered or amorphous. Therefore, it could be speculated that an effective interaction existed between CBD and CDs in the inclusion complexes, which demonstrated that CBD had been entrapped into the cavity of CDs. Further experiments should be accomplished to confirm that CBD/β-CD IC and CBD/DM-β-CD IC were successfully prepared.

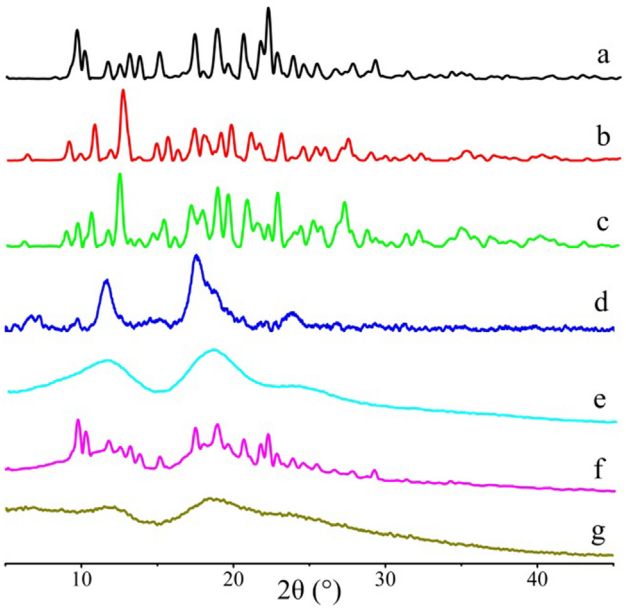

Fig. 5. PXRD patterns of (a) CBD, (b) β-CD, (c) physical mixture (PM) of CBD and β-CD, (d) CBD/β-CD IC, (e) DM-β-CD, (f) PM of CBD and DM-β-CD, and (g) CBD/DM-β-CD IC.

3.5.2. FT-IR analysis

FT-IR method can recognize the changes of characteristic peak position, frequency, and shape of many groups in a molecule. Therefore, it is widely employed to study the host–guest interaction in inclusion complexes [47]. If CBD forms the inclusion complexes with CDs, the characteristic peaks of CBD probably shift, decrease, or disappear. The FT-IR spectra of CBD, β-CD, DM-β-CD, their physical mixtures, and inclusion complexes were shown in Fig. 6. The spectrum of CBD exhibited two significant characteristic bands at 3520 cm^{-1} and 3441 cm^{-1} corresponding to the stretching vibration of hydroxyl groups, peak at 3073 cm^{-1} assigned to the C—H stretching vibration of the benzene ring, at 2964 cm^{-1}, 2924 cm^{-1}, 2854 cm^{-1}, and 2828 cm^{-1} denoted for the stretching vibration of methyl and methylene groups, at 1623 cm^{-1}, 1581 cm^{-1}, 1513 cm^{-1}, and 1443 cm^{-1} corresponding to benzene skeleton vibration, at 1375 cm^{-1} denoted for the bending vibration of methyl groups, and at 1214 cm^{-1} for the C—O stretching vibra-

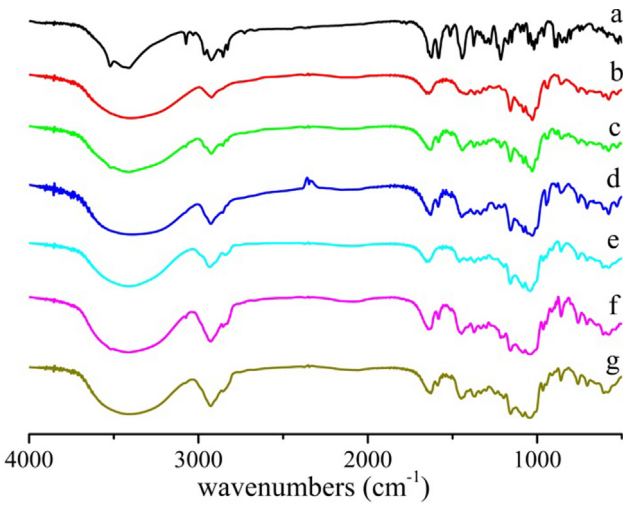

Fig. 6. FT-IR spectra of (a) CBD, (b) β-CD, (c) PM of CBD and β-CD, (d) CBD/β-CD IC, (e) DM-β-CD, (f) PM of CBD and DM-β-CD, and (g) CBD/DM-β-CD IC.

tion. For β-CD, the broad band at 3405 cm^{-1} was denoted for the stretching vibration of hydroxyl groups. The peak at 2923 cm^{-1} was assigned to the stretching vibration of C—H, and some other remarkable peaks at 1654 cm^{-1}, 1158 cm^{-1}, 1031 cm^{-1} were corresponding to H—O—H bending vibration, C—O stretching vibration, and C—O—C stretching vibration, respectively. For DM-β-CD, the spectrum was very similar to that of β-CD, except for one more significant peak at 2840 cm^{-1} for the stretching vibration of methyl groups. Like the PXRD patterns, the FT-IR spectra of the physical mixtures were also presented as a simple superposition of CBD and CDs, suggesting no interaction between CBD and CDs when they were mixed physically. It was worth noting that the spectra of CBD/β-CD IC and CBD/DM-β-CD IC were similar to those of CDs because of the low content of CBD in the inclusion complexes. Meanwhile, the characteristic peaks of CBD at 3520 cm^{-1}, 3073 cm^{-1}, 2964 cm^{-1}, 2828 cm^{-1}, and 1214 cm^{-1} were all disappeared nearly. The findings showed that CBD had entirely or partly entered the cavity of the CDs, resulting in that the vibration of the above-mentioned groups was restricted. These results further proved that CBD/β-CD IC and CBD/DM-β-CD IC were successfully formed.

3.5.3. DSC analysis

DSC analysis which is a common method to study the physical states of inclusion complexes, was used to investigate the inclusion complexes of CBD with CDs. The DSC thermograms showed in Fig. 7 displayed that CBD exhibited a sharp endothermic peak at its melting point (66 °C) and a small endothermic peak at 259 °C due to a phase transformation. The DSC curves of β-CD and DM-β-CD were both characterized by a very wide endothermic band between 50 °C and 125 °C attributed to dehydration. Moreover, the DSC curve of DM-β-CD also displayed a large endothermic peak at 265 °C because of a phase transformation. On the other hand, the DSC thermograms of the physical mixtures were similar to the superposition of the individual curves of them, although the peaks of CBD were smaller. However, the peaks of CBD almost disappeared in the DSC curves of CBD/β-CD IC and CBD/DM-β-CD IC. Furthermore, the peak at 265 °C of DM-β-CD shifted significantly in CBD/DM-β-CD IC, which indicated an interaction between CBD and DM-β-CD. Therefore, combined with the findings of PXRD and FT-IR, it was proved that CBD/β-CD IC and CBD/DM-β-CD IC had been successfully prepared.

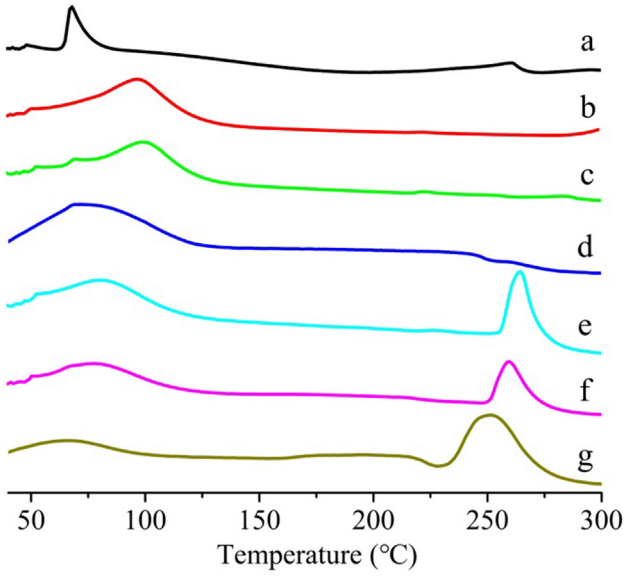

Fig. 7. DSC thermograms of (a) CBD, (b) β-CD, (c) PM of CBD and β-CD, (d) CBD/β-CD IC, (e) DM-β-CD, (f) PM of CBD and DM-β-CD, and (g) CBD/DM-β-CD IC.

3.5.4. SEM analysis

SEM is generally employed as an auxiliary method to verify the formation of inclusion complexes and observe their morphology before and after inclusion [48]. The SEM images of these samples were displayed in Fig. 8. CBD was crystalline with a nubby shape of different sizes. β-CD exhibited a prismatic crystal structure of different sizes, while DM-β-CD was a near-spherical shape with cavity or cavity fragment structure. On the other hand, the physical mixtures showed the combination of CBD crystal structure and CDs structures, indicating no change in the morphology of the host and guest molecules and no interaction between them. However, the images of the inclusion complexes were completely different from those of the physical mixtures. In the inclusion complexes, the characteristic structures of CBD and CDs disappeared completely. Both CBD/β-CD IC and CBD/DM-β-CD IC displayed a homogeneous irregular blocky structure. These findings were consistent with the conclusions of PXRD, FT-IR, and DSC, from the side confirming that the inclusion complexes were successfully formed.

3.5.5. ^1H NMR analysis

To explore the characteristics of the inclusion complexes, the ^1H NMR spectra of CBD, CDs, their physical mixtures, and inclusion complexes were analyzed. As shown in Figs. 9, 1H NMR of CBD, 600 MHz, DMSO d_6: δ_H 0.86 (3H, H-15 of CBD), δ_H 1.26 (4H, H-13, 14 of CBD), δ_H 1.47 (2H, H-12 of CBD), δ_H 1.59 (6H, H-6, 7 of CBD), δ_H 1.65 (2H, H-2 of CBD), δ_H 1.92–2.10 (2H, H-1 of CBD), δ_H 2.30 (2H, H-11 of CBD), δ_H 2.49 (solvent peak), δ_H 3.03 (1H, H-3 of CBD), δ_H 3.33 (water peak), δ_H 3.83 (1H, H-4 of CBD), δ_H 4.41–4.49 (2H, H-8 of CBD), δ_H 5.08 (1H, H-5 of CBD), δ_H 6.01 (2H, H-9, 10 of CBD), and δ_H 8.63 (2H, —OH of CBD), respectively, were all exactly detected.

If a guest molecule is entrapped into the cavity of CDs, the chemical environment over the protons (H-3 and H-5), which are inside the cavity of CDs, will be transformed. Then the chemical shifts of the protons will be changed, while that of the protons (H-1, H-2, and H-4) which are outside the cavity will stay the same as before. Furthermore, the chemical shifts of the protons belonging to the guest molecule will be changed after encapsulation as well [49]. Therefore, to analyze the interaction between CBD and CDs, the chemical shift in the ^1H NMR spectra of CBD, β-CD, DM-β-CD, and their inclusion complexes were compared. Nevertheless, all the values of $\Delta\delta$ were ≤ 0.02 (data not shown in the article), suggesting that the effects due to the inclusion processes on the chemical shifts of CBD and CDs were negligible. These results were similar to the findings of Yao et al. [50]. The reason for the insignificant change in chemical shifts might be due to the weak non-covalent forces between CBD and the CDs. So next, molecular docking was used to simulate the structures of the inclusion complexes.

3.6. Molecular docking

The possible conformations of the inclusion complexes were determined through molecular docking. Fig. 10 represented the molecular structures of CBD/β-CD IC and CBD/DM-β-CD IC with the lowest docking energy. According to the docking results, there was no doubt that CBD was embedded in the cavity of the CDs, suggesting that CBD could form inclusion complexes with β-CD or DM-β-CD theoretically. As shown in Fig. 10(a), the CBD molecule was not entrapped into the cavity of β-CD completely, but its hydrophobic ring, which was close to the narrow side of β-CD, was thoroughly encapsulated into the cavity of β-CD. However, Fig. 10(b) presented a different structure. The alkyl chain of CBD penetrated the cavity of DM-β-CD and was close to the narrow side

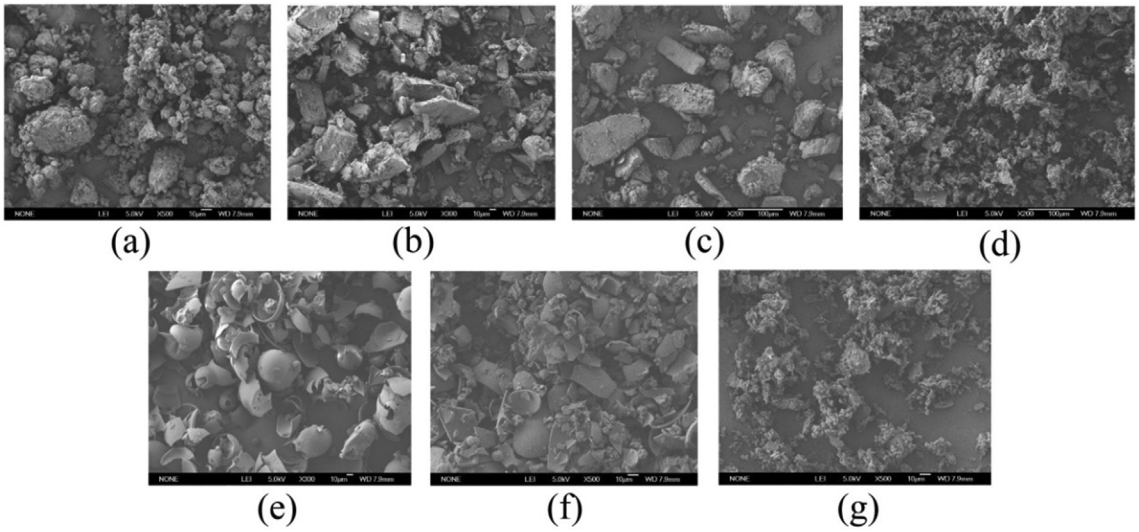

Fig. 8. SEM images of (a) CBD, (b) β-CD, (c) PM of CBD and β-CD, (d) CBD/β-CD IC, (e) DM-β-CD, (f) PM of CBD and DM-β-CD, and (g) CBD/DM-β-CD IC.

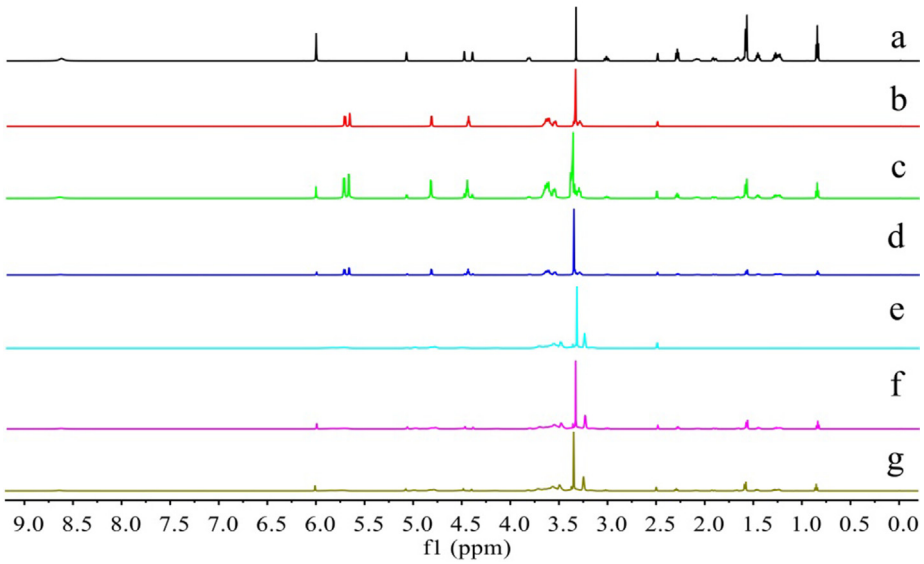

Fig. 9. ^{1}H NMR spectra of (a) CBD, (b) β-CD, (c) PM of CBD and β-CD, (d) CBD/β-CD IC, (e) DM-β-CD, (f) PM of CBD and DM-β-CD, and (g) CBD/DM-β-CD IC in DMSO d_6.

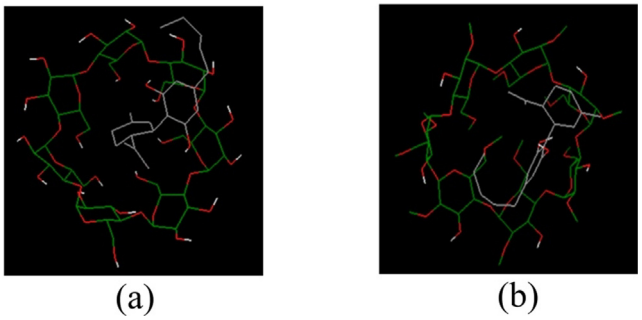

Fig. 10. Molecular docking of the lowest docking energy conformation of (a) CBD with β-CD and (b) CBD with DM-β-CD.

of DM-β-CD, while the hydrophobic ring of CBD was located at the wide side of DM-β-CD.

Besides, the interaction energy of the inclusion complexes was calculated. As shown in Table 3, the torsional energy of the two complexes was equal, while the intermolecular energy, internal energy, and unbound energy were different because of substitution. As a result, the binding energy of CBD/DM-β-CD IC was lower than that of CBD/β-CD IC, indicating that CBD/DM-β-CD IC was more stable than CBD/β-CD IC. This finding was consistent with the results of the phase solubility study.

3.7. Water solubility study

The water solubility of CBD in the inclusion complexes with β-CD or DM-β-CD was evaluated by preparing their saturated aqueous solutions. Table 4 showed the water solubility of CBD in CBD/β-CD IC and CBD/DM-β-CD IC. The water solubility of CBD was significantly increased to 0.395 and 14.118 μg/mL, which was promoted by 17-fold and 614-fold respectively, as compared with that of raw CBD (0.023 μg/mL). As mentioned above, the outer surface of CD is hydrophilic while the inner cavity which can accommodate CBD is hydrophobic. And hydrophobic CBD could interact with the cavity of CD by intermolecular hydrogen bonds

Table 3
The lowest energy values for CBD/β-CD IC and CBD/DM-β-CD IC based on Autodock results.

	Intermolecular Energy (kcal/mol)	Internal Energy (kcal/mol)	Torsional Energy (kcal/mol)	Unbound Energy (kcal/mol)	Binding Energy [a] (kcal/mol)
β-CD	−8.18	−1.40	2.39	−1.40	−5.80
DM-β-CD	−9.61	−1.67	2.39	−1.67	−7.22

[a] Binding Energy = Intermolecular Energy + Internal Energy + Torsional Energy−Unbound Energy.

Table 4
The water solubility of CBD in the form of inclusion complexes at 37 °C.

	Water solubility of CBD (μg/mL)	Fold increase than raw CBD
CBD/β-CD IC	0.395	17
CBD/DM-β-CD IC	14.118	614
raw CBD	0.023	1

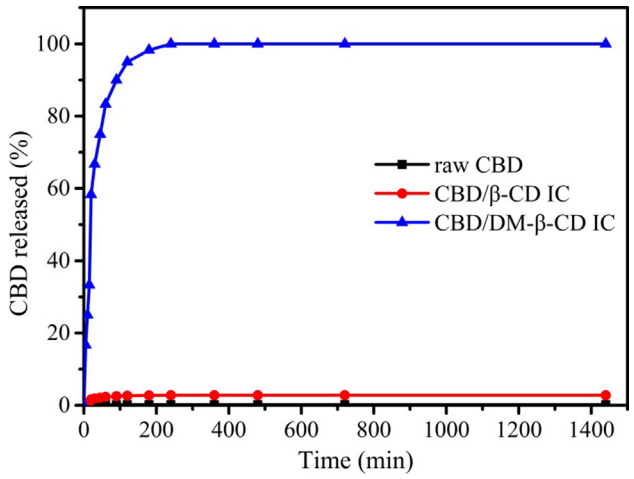

Fig. 11. In vitro dissolution profiles of raw CBD, CBD/β-CD IC, and CBD/DM-β-CD IC at 37 °C.

and Van der Waals force. Therefore, the solubility of CBD could be improved by using the water-soluble CD as a drug carrier. The water solubility of CBD in CBD/DM-β-CD IC was better than that in CBD/β-CD IC because of the higher water solubility and more suitable cavity of DM-β-CD than β-CD [31]. It also should be noted that the LE of the two inclusion complexes was 20.4% and 17.7% respectively, as mentioned above. To the best of our knowledge, there is still no report about a 600-fold increase in solubility of CBD at such a high loading efficiency.

3.8. In vitro dissolution study

In vitro dissolution study simulates the amount of drug released in the selected dissolution medium at predetermined time intervals. The in vitro dissolution profiles of raw CBD, CBD/β-CD IC, and CBD/DM-β-CD IC were displayed in Fig. 11. The dissolution rate of raw CBD was very low even after one day. This should be associated with the poor aqueous solubility of CBD, which was not encapsulated to increase its water solubility. In contrast, both the two inclusion complexes showed a higher dissolution rate than raw CBD. CBD/β-CD IC released 1.9% of CBD after 30 min and achieved the maximum dissolution of 2.8% at 180 min, while CBD/DM-β-CD IC released 66.7% of CBD after 30 min and nearly released all CBD molecules at 240 min. The dissolution performance of CBD/DM-β-CD IC was greatly better than that of CBD/β-CD IC. The high dissolution rate of CBD/DM-β-CD IC could be attributed to the high water solubility of DM-β-CD. When CBD/DM-β-CD IC was dissolved in water, a large number of water molecules would occupy the position of CBD in the cavity, resulting in that the interaction between CBD and DM-β-CD changed weaker. On the other hand, the structure of DM-β-CD might burst because of swelling by absorption of water molecules, and then CBD was released from DM-β-CD. Therefore, CBD/DM-β-CD IC had a high dissolution rate [51,52]. The in vitro dissolution results were in agreement with the physicochemical and morphological characterizations mentioned above, confirming the formation of the inclusion complexes, which improved the solubility property of CBD.

3.9. Antioxidant activity study

The antioxidant activity of CBD and its inclusion complexes were estimated by ABTS and DPPH free radical scavenging assays. As shown in Fig. 12(a), raw CBD and its inclusion complexes could

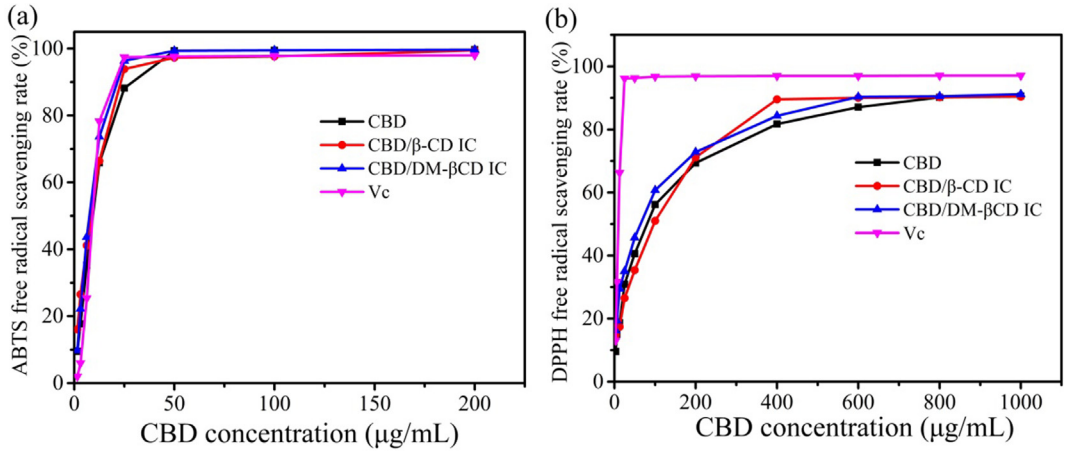

Fig. 12. (a) ABTS and (b) DPPH free radical scavenging activity of raw CBD, CBD/β-CD IC, and CBD/DM-β-CD IC. Vc was used as a positive control.

effectively scavenge ABTS free radical. Besides, the ABTS free radical scavenging rate increased with the increasing concentration of CBD or the inclusion complexes. And when the concentration of CBD or the inclusion complexes solutions reached a high degree, the scavenging rate tended to be stable. In particular, at low concentration, the scavenging activity of the inclusion complexes was more potent than that of raw CBD. The calculated EC_{50} for ABTS free radical exhibited that the scavenging activity of CBD/β-CD IC (8.5 μg/mL) and CBD/DM-β-CD IC (7.6 μg/mL) was significantly better than that of raw CBD (9.4 μg/mL), even stronger than that of Vc (9.2 μg/mL). As shown in Fig. 12(b), raw CBD and its inclusion complexes also could effectively scavenge DPPH free radical. The changing trend of scavenging rate was consistent with that of ABTS free radical. The calculated EC_{50} for DPPH free radical showed that the scavenging activity of CBD/DM-β-CD IC (65 μg/mL) was stronger than that of raw CBD (80 μg/mL). The ABTS and DPPH radical scavenging ability of a molecule was reported to be closely related to its hydrogen-donating ability [53]. Therefore, the results indicated that the complexation might promote the hydrogen donation of CBD, which was likely associated with the new conformation of CBD in the inclusion complexes and the hydrogen bonds formed between CBD and the CDs that made the hydrogen in the hydroxyl groups of CBD release more easily [40]. The results were consistent with some studies which had reported the stronger antioxidant activity of inclusion complexes compared with raw compounds, such as myricetin [50], tertiary butylhydroquinone [47], and oligopeptides [54]. Valh et al. [55] also reported that the antioxidant of CBD was promoted by microencapsulation in liposomes, although the results were not significant. Besides, a synergistic effect was reported between CBD and THC regarding their antioxidant activity, which could improve the antioxidant activity of CBD effectively [56]. In conclusion, these findings indicated that the antioxidant activity of CBD was not eliminated after forming inclusion complexes, but stronger than that of its raw state.

4. Conclusions

This work showed that CBD formed inclusion complexes with β-CD and DM-β-CD at a 1:1 stoichiometric ratio based on phase solubility study and Job's plot. The thermodynamics analysis demonstrated that the inclusion process was spontaneous and endothermic. Then, CBD/β-CD IC and CBD/DM-β-CD IC were prepared and systematically characterized by PXRD, FT-IR, DSC, SEM, and ^{1}H NMR, which suggested that CBD was transformed from crystalline to amorphous state after encapsulation. Moreover, molecular docking further revealed that CBD was encapsulated successfully. The following experiments displayed that the water solubility of CBD in CBD/β-CD IC and CBD/DM-β-CD IC was significantly enhanced by 17-fold and 614-fold respectively at a high loading efficiency, and the in vitro dissolution performance of CBD was also improved after complexation. Besides, the antioxidant activity of CBD was enhanced to some extent after forming inclusion complexes with β-CD and DM-β-CD. It was worth noting that the ABTS radical scavenging ability of the inclusion complexes was stronger than that of Vc. In brief, this work provided theoretical and experimental support for expanding the application of CBD in the food and daily chemical industry. However, the release behavior and antioxidant activity of the inclusion complexes in vivo are still unclear, so further researches are required to clarify these questions.

CRediT authorship contribution statement

Hang Li: Data curation, Investigation, Methodology, Writing - original draft. **Sen-Lin Chang:** Investigation, Methodology. **Tan-Ran Chang:** Investigation, Methodology. **Ying You:** Investigation, Methodology. **Xiao-Dong Wang:** Investigation, Writing - review & editing. **Li-Wei Wang:** Investigation, Writing - review & editing. **Xiao-Fan Yuan:** Investigation, Writing - review & editing. **Ming-Hui Tan:** Methodology. **Pei-Dong Wang:** Methodology. **Peng-Wei Xu:** Methodology. **Wei-Bo Gao:** Investigation. **Qing-Sheng Zhao:** Investigation, Writing - review & editing. **Bing Zhao:** Investigation, Project administration.

Declaration of Competing Interest

The authors declare that they have no known competing financial interests or personal relationships that could have appeared to influence the work reported in this paper.

Acknowledgments

This work was financially supported by Yunnan Hempmon Pharmaceutical Co., Ltd.

References

[1] A.A. Izzo, F. Borrelli, R. Capasso, V. Di Marzo, R. Mechoulam, Non-psychotropic plant cannabinoids: new therapeutic opportunities from an ancient herb, Trends Pharmacol. Sci. 30 (2009) 515–527.
[2] M. Elbaz, M.W. Nasser, J. Ravi, N.A. Wani, D.K. Ahirwar, H. Zhao, S. Oghumu, A. R. Satoskar, K. Shilo, W.E. Carson III, R.K. Ganju, Modulation of the tumor microenvironment and inhibition of EGF/EGFR pathway: novel anti-tumor mechanisms of cannabidiol in breast cancer, Mol. Oncol. 9 (2015) 906–919.
[3] R. Stukelj, M. Bencina, M. Fanetti, M. Valant, M. Drab, A. Iglic, V. Kralj-Iglic, Synthesis of stable cannabidiol (CBD) nanoparticles in suspension, Mater. Tehnol. 53 (2019) 543–549.
[4] S. Atalay, I. Jarocka-Karpowicz, E. Skrzydlewska, Antioxidative and anti-Inflammatory properties of cannabidiol, Antioxidants 9 (2020) 20.
[5] L.D. Martinenghi, R. Jonsson, T. Lund, H. Jenssen, Isolation, purification, and antimicrobial characterization of cannabidiolic acid and cannabidiol from cannabis sativa L, Biomolecules 10 (2020) 15.
[6] X. Zhang, Y. Qin, Z.H. Pan, M.J. Li, X.N. Liu, X.Y. Chen, G.W. Qu, L. Zhou, M.L. Xu, Q.S. Zheng, D.F. Li, Cannabidiol induces cell cycle arrest and cell apoptosis in human gastric cancer SGC-7901 cells, Biomolecules 9 (2019) 17.
[7] B. Kis, F.C. Ifrim, V. Buda, S. Avram, I.Z. Pavel, D. Antal, V. Paunescu, C.A. Dehelean, F. Ardelean, Z. Diaconeasa, C. Soica, C. Danciu, Cannabidiol-from plant to human body: a promising bioactive molecule with multi-target effects in cancer, Int. J. Mol. Sci. 20 (2019) 24.
[8] L.R. Motadi, S. Lukhelo, Isolated cannabidiol from cannabis sativa plant extracts inhibit growth and induce apoptosis in cervical cancer cells, Cancer Res. 76 (2016) 3.
[9] S. Burstein, Cannabidiol (CBD) and its analogs: a review of their effects on inflammation, Bioorg. Med. Chem. 23 (2015) 1377–1385.
[10] C. Xu, T.R. Chang, Y.Q. Du, C.H. Yu, X. Tan, X.D. Li, Pharmacokinetics of oral and intravenous cannabidiol and its antidepressant-like effects in chronic mild stress mouse model, Environ. Toxicol. Pharmacol. 70 (2019) 7.
[11] Y.L. Huang, T. Wan, N.Z. Pang, Y.J. Zhou, X.Y. Jiang, B.Y. Li, Y.Y. Gu, Y.F. Huang, X. D. Ye, H. Lian, Z.F. Zhang, L.L. Yang, Cannabidiol protects livers against nonalcoholic steatohepatitis induced by high-fat high cholesterol diet via regulating NF-kappa B and NLRP3 inflammasome pathway, J. Cell. Physiol. 234 (2019) 21224–21234.
[12] A. Gegotek, S. Atalay, P. Domingues, E. Skrzydlewska, Proteomic analysis of cannabidiol effect on human skin fibroblasts exposed to UVA or UVB irradiation, Free Radic. Biol. Med. 139 (2019), S27 S27.
[13] G.H. Briggs, Cannabidiol, a non-psychoactive marijuana component, exhibits antioxidant and neuroprotective effects in neuronal Alzheimer's cell model SH-5Y, Faseb J. 32 (2018) 1.
[14] G. Calapai, C. Mannucci, I. Chinou, L. Cardia, F. Calapai, E.E. Sorbara, B. Firenzuoli, V. Ricca, G.F. Gensini, F. Firenzuoli, Preclinical and clinical evidence supporting use of cannabidiol in psychiatry, Evid.-Based Complement Altern Med. (2019) 11.
[15] S. Bonaccorso, A. Ricciardi, C. Zangani, S. Chiappini, F. Schifano, Cannabidiol (CBD) use in psychiatric disorders: a systematic review, Neurotoxicology 74 (2019) 282–298.
[16] G.M. Mandolini, M. Lazzaretti, A. Pigoni, L. Oldani, G. Delvecchio, P. Brambilla, Pharmacological properties of cannabidiol in the treatment of psychiatric disorders: a critical overview, Epidemiol. Psychiatr. Sci. 27 (2018) 327–335.
[17] D.S. Reddy, The utility of cannabidiol in the treatment of refractory epilepsy, Clin. Pharmacol. Ther. 101 (2017) 182–184.
[18] K.A. Jadoon, S.H. Ratcliffe, D.A. Barrett, E.L. Thomas, C. Stott, J.D. Bell, S.E. O'Sullivan, G.D. Tan, Efficacy and safety of cannabidiol and tetrahydrocannabivarin on glycemic and lipid parameters in patients with

type 2 diabetes: a randomized, double-blind, placebo-controlled, parallel group pilot study, Diabetes Care 39 (2016) 1777–1786.
[19] E.J. Carrier, J.A. Auchampach, C.J. Hillard, Inhibition of an equilibrative nucleoside transporter by cannabidiol: a mechanism of cannabinoid immunosuppression, Proc. Natl. Acad. Sci. U. S. A. 103 (2006) 7895–7900.
[20] Epidiolex. Full Prescribing Information, Greenwich Biosciences Inc. 2018. https://www.accessdata.fda.gov/drugsatfda_docs/label/2018/210365lbl.pdf, 2020 (accessed 10 April 2020).
[21] S. Song, K. Gao, R.M. Niu, W.L. Yi, J.H. Zhang, C.Z. Gao, B. Yang, X.L. Liao, Binding behavior, water solubility and in vitro cytotoxicity of inclusion complexes between ursolic acid and amino-appended beta-cyclodextrins, J. Mol. Liq. 296 (2019) 9.
[22] F. Fateminasab, A.K. Bordbar, S. Shityakov, A.A. Saboury, Molecular insights into inclusion complex formation between beta- and gamma-cyclodextrins and rosmarinic acid, J. Mol. Liq. 314 (2020) 16.
[23] A. Matencio, F. Garcia-Carmona, J.M. Lopez-Nicolas, The inclusion complex of oxyresveratrol in modified cyclodextrins: a thermodynamic, structural, physicochemical, fluorescent and computational study, Food Chem. 232 (2017) 177–184.
[24] Y. Zheng, I.S. Haworth, Z. Zuo, M.S.S. Chow, A.H.L. Chow, Physicochemical and structural characterization of quercetin-beta-cyclodextrin complexes, J. Pharm. Sci. 94 (2005) 1079–1089.
[25] V. Buko, I. Zavodnik, B. Palecz, A. Stepniak, S. Kirko, A. Shlyahtun, W. Misiuk, E. Belonovskaya, O. Lukivskaya, E. Naruta, I. Kuzmitskaya, T. Ilyich, B. Erdenebayar, S. Rakhmadieva, Betulin/2-hydroxypropyl-beta-cyclodextrin inclusion complex: physicochemical characterization and hepatoprotective activity, J. Mol. Liq. 309 (2020) 10.
[26] N. Li, N. Wang, T.N. Wu, C.L. Qiu, X.T. Wang, S.H. Jiang, Z. Zhang, T. Liu, C.L. Wei, T. Wang, Preparation of curcumin-hydroxypropyl-beta-cyclodextrin inclusion complex by cosolvency-lyophilization procedure to enhance oral bioavailability of the drug, Drug Dev. Ind. Pharm. 44 (2018) 1966–1974.
[27] L. Szente, J. Szejtli, Cyclodextrins as food ingredients, Trends Food Sci. Technol. 15 (2004) 137–142.
[28] P. Lv, D.J. Zhang, M.B. Guo, J. Liu, X. Chen, R. Guo, Y.P. Xu, Q.Y. Zhang, Y. Liu, H.Y. Guo, M. Yang, Structural analysis and cytotoxicity of host-guest inclusion complexes of cannabidiol with three native cyclodextrins, J. Drug Deliv. Sci. Technol. 51 (2019) 337–344.
[29] J. Mannila, T. Jarvinen, K. Jarvinen, P. Jarho, Precipitation complexation method produces cannabidiol/beta-cyclodextrin inclusion complex suitable for sublingual administration of cannabidiol, J. Pharm. Sci. 96 (2007) 312–319.
[30] Z. Lu, B. Cheng, Y.L. Hu, Y.H. Zhang, G.L. Zou, Complexation of resveratrol with cyclodextrins: solubility and antioxidant activity, Food Chem. 113 (2009) 17–20.
[31] C. Jullian, C. Cifuentes, M. Alfaro, S. Miranda, G. Barriga, C. Olea-Azar, Spectroscopic characterization of the inclusion complexes of luteolin with native and derivatized beta-cyclodextrin, Bioorg. Med. Chem. 18 (2010) 5025–5031.
[32] Y.P. Wu, Y. Xiao, Y.X. Yue, K. Zhong, Y.L. Zhao, H. Gao, A deep insight into mechanism for inclusion of 2R,3R-dihydromyricetin with cyclodextrins and the effect of complexation on antioxidant and lipid-lowering activities, Food Hydrocolloids 103 (2020) 9.
[33] L.N. Dong, M. Liu, A.J. Chen, Y. Wang, D.Z. Sun, Solubilities of quercetin in three beta-cyclodextrin derivative solutions at different temperatures, J. Mol. Liq. 177 (2013) 204–208.
[34] T. Higuchi, K.A. Connors, Phase solubility techniques, Adv. Anal. Chem. Instrum. 4 (1965) 117–212.
[35] P. Job, Formation and stability of inorganic complexes in solution, Ann. Chim. Phys. 9 (1928) 113–203.
[36] S. Cosconati, S. Forli, A.L. Perryman, R. Harris, D.S. Goodsell, A.J. Olson, Virtual screening with AutoDock: theory and practice, Expert. Opin. Drug Discov. 5 (2010) 597–607.
[37] N. Nenadis, L.F. Wang, M. Tsimidou, H.Y. Zhang, Estimation of scavenging activity of phenolic compounds using the ABTS.+ assay, J. Agric. Food Chem. 52 (2004) 4669–4674.
[38] R.L. Prior, X. Wu, K. Schaich, Standardized methods for the determination of antioxidant capacity and phenolics in foods and dietary supplements, J. Agric. Food Chem. 53 (2005) 4290–4302.
[39] C. Cannava, V. Crupi, M. Guardo, D. Majolino, R. Stancanelli, S. Tommasini, C.A. Ventura, V. Venuti, Phase solubility and FTIR-ATR studies of idebenone/sulfobutyl ether beta-cyclodextrin inclusion complex, J. Incl. Phenom. Macrocycl. Chem. 75 (2013) 255–262.
[40] T.A. Nguyen, B. Liu, J. Zhao, D.S. Thomas, J.M. Hook, An investigation into the supramolecular structure, solubility, stability and antioxidant activity of rutin/cyclodextrin inclusion complex, Food Chem. 136 (2013) 186–192.
[41] Q. Zhou, X. Wei, W. Dou, G. Chou, Z. Wang, Preparation and characterization of inclusion complexes formed between baicalein and cyclodextrins, Carbohydr. Polym. 95 (2013) 733–739.
[42] C. Desai, B. Prabhakar, Nano-amorphous composites of cilostazol–HP-β-CD inclusion complexes: physicochemical characterization, structure elucidation, thermodynamic studies and in vitro evaluation, J. Incl. Phenom. Macrocycl. Chem. 81 (2015) 175–191.
[43] Y. Matsui, K. Mochida, Binding forces cntributing to the association of cyclodextrin with alcohol in an aqueous solution, B. Chem. Soc. Jpn. 52 (1979) 2808–2814.
[44] S. Paul, P.W.S. Heng, L.W. Chan, pH-dependent complexation of hydroxypropyl-beta-cyclodextrin with chlorin e6: effect on solubility and aggregation in relation to photodynamic efficacy, J. Pharm. Pharmacol. 68 (2016) 439–449.
[45] B.D. Lima, C.D. Campos, A. Santos, V.C.N. Santos, G. Trindade, S. Shanmugam, E. W.M. Pereira, R.N. Marreto, M.C. Duarte, J. Almeida, J.D.S. Quintans, L.J. Quintans, A.A.D. Araujo, Development of morin/hydroxypropyl-beta-cyclodextrin inclusion complex: enhancement of bioavailability, antihyperalgesic and anti-inflammatory effects, Food Chem. Toxicol. 126 (2019) 15–24.
[46] A. Praveena, S. Prabu, R. Rajamohan, Encapsulation of quercetin in beta-cyclodextrin and (2-hydroxypropyl)-beta-cyclodextrin cavity: in-vitro cytotoxic evaluation, J. Macromol. Sci. Part A-Pure Appl. Chem. 54 (2017) 894–901.
[47] H.Y. Pu, Q.M. Sun, P.X. Tang, L.D. Zhao, Q. Li, Y.Y. Liu, H. Li, Characterization and antioxidant activity of the complexes of tertiary butylhydroquinone with beta-cyclodextrin and its derivatives, Food Chem. 260 (2018) 183–192.
[48] B. Liu, W. Li, J. Zhao, Y. Liu, X. Zhu, G. Liang, Physicochemical characterisation of the supramolecular structure of luteolin/cyclodextrin inclusion complex, Food Chem. 141 (2013) 900–906.
[49] C. Yuan, Z. Jin, X. Xu, Inclusion complex of astaxanthin with hydroxypropyl-β-cyclodextrin: UV, FTIR, 1H NMR and molecular modeling studies, Carbohydr. Polym. 89 (2012) 492–496.
[50] Y.S. Yao, Y. Xie, C. Hong, G.W. Li, H.Y. Shen, G. Ji, Development of a myricetin/hydroxypropyl-beta-cyclodextrin inclusion complex: preparation, characterization, and evaluation, Carbohydr. Polym. 110 (2014) 329–337.
[51] K. Kaur, R. Jindal, D. Jindal, Synthesis, characterization and studies on host-guest interactions of inclusion complexes of metformin hydrochloride with beta-cyclodextrin, J. Mol. Liq. 282 (2019) 162–168.
[52] M. Ahmad, A. Gani, Ultrasonicated resveratrol loaded starch nanocapsules: Characterization, bioactivity and release behaviour under in-vitro digestion, Carbohydr. Polym. 251 (2021) 8.
[53] J. Yang, J. Guo, J. Yuan, In vitro antioxidant properties of rutin, LWT - Food Science and Technology 41 (2008) 1060–1066.
[54] J. Li, S. Geng, Y. Wang, Y. Lv, H. Wang, B. Liu, G. Liang, The interaction mechanism of oligopeptides containing aromatic rings with β-cyclodextrin and its derivatives, Food Chem. 286 (2019) 441–448.
[55] J.V. Valh, Z. Persin, B. Voncina, K. Vrezner, L. Tusek, L.F. Zemljic, Microencapsulation of Cannabidiol in Liposomes as Coating for Cellulose for Potential Advanced Sanitary Material, Coatings 11 (2021) 18.
[56] A.C.M. Hacke, D. Lima, F. de Costa, K. Deshmukh, N. Li, A.M. Chow, J.A. Marques, R.P. Pereira, K. Kerman, Probing the antioxidant activity of Delta(9)-tetrahydrocannabinol and cannabidiol in Cannabis sativa extracts, Analyst 144 (2019) 4952–4961.